'Breathing-Crystals'
The Origin of Electrochemical Activity of Mesoporous Li-MnO2

Thi X.T. Sayle,[1,2] Kenneth Kgatwane,[2] Phuti E. Ngoepe[2] and Dean C. Sayle[1,*]
[1] School of Physical Sciences, University of Kent, Canterbury, CT2 7NZ, UK
[*]d.c.sayle@kent.ac.uk
[2] Materials Modelling Centre, University of Limpopo, Private Bag x1106, Sovenga, 0727, South Africa.

ABSTRACT: Akin to Le Chatalier's principle, we show that a mesoporous material can mitigate the effect of stress by expanding or contracting elastically into the pore space; we simulate this 'breathing-crystal' phenomenon using MD simulation. In particular, our simulations reveal that mesoporous Li-MnO2 is electrochemically active because the stress, associated with charge cycling, does not influence the structure or dimensions of the (unlithiated) 1x1 tunnels in which the lithium ions intercalate and reside. Conversely, the parent bulk material suffers structural collapse and blockage of the 1x1 tunnels under stress. The mechanism associated with Li deintercalation is presented together with the activation energy barriers, which are calculated to be 0.4eV - irrespective of whether the mesoporous host is unstrained or under considerable (1.6 GPa) tensile or compressive stress.

INTRODUCTION

Mesoporous β-MnO_2, which conforms to the pyrolocite crystal structure and is isostructural with rutile-TiO_2, can act as a host lattice for the intercalation, storage and deintercalation of lithium ions during charge cycling and can be exploited as an electrode in Li-ion battery systems.[1,2,3,4,5] In particular, the β-MnO_2 crystal structure comprises 1x1 tunnels, fig 1, that are able to accommodate the Li ions and facilitate their transport within the material via diffusion along these tunnels.[6] During charge/discharge cycling, the lithium ions are able to enter the surfaces of the internal pores of the mesoporous β-MnO_2 and move into the 1x1 tunnels. Conversely, the parent bulk material is electrochemically inactive.[7]

When Li is intercalated into the mesoporous β-MnO_2 host lattice, it induces considerable stress. In particular, it has been shown that the lattice parameters change from a = 4.40 Å, c = 2.88 Å for (unlithiated) mesoporous β-MnO_2 to a = 5.01 Å, c = 2.81 Å for mesoporous $Li_{0.92}MnO_2$-β.7 As regions of β-MnO_2 expand during lithiation, they will impart stress upon neighbouring (unlithiated) regions of the material. In particular, considerable stress-induced deformation, associated with Li intercalation, has been reported with atom level resolution.[8] Nanostructuring can help mitigate the effect of stress associated with Li intercalation.[9] To help explain why mesoporous β-MnO_2 is electrochemically active, in contrast to the parent bulk material, we simulate the effect of stress on both mesoporous and bulk β-MnO_2. We focus especially on the effect that stress has on the structure and dimensions of the 1x1 network of tunnels, in which the Li ions reside, and the surface 'exit sites' through which Li deintercalates. Atomistic simulation of battery systems has been shown to provide valuable insight to inform experimentation.[10]

Our second area of exploration is the intercalation/deintercalation of Li into the host lattice. Thompsett and co-workers used Density Functional Theory (DFT) to predict the crystal morphology of β-MnO_2 and the structure of exposed surfaces by the material.[11] This is important because Li intercalation/deintercalation will occur at such surfaces; the energetics of which will govern the electrochemical properties of the material.[12] The predicted equilibrium morphology, based upon calculated surface energies, comprised {110}, {211} and {001} surfaces. We note that only {001} surfaces proffers 1x1 tunnels that are perpendicular to the surface. Moreover, Thompsett and co-workers calculated, using DFT+U, that the activation energy barriers, associated with Li ion mobility from the bulk to the surface is 0.6 and 0.3eV for the (101) and (001) surfaces respectively. However, based upon the predicted equilibrium morphology, 'access to the route of facile c-axis migration (along the 1x1 tunnels) is only available at the (101) and symmetry equivalent surfaces and it is likely that this is the surface through which most lithium must migrate into the bulk crystal.' The authors conclude that 'such (high) activation energy barrier for Li intercalation via the (101) surface (0.6 eV) is likely to limit the practical use of bulk samples.' The authors proffer that nanostructuring might facilitate facile intercalation/deintercalation because the high curvature of the mesoporous β-MnO_2 will facilitate the exposure of alternative surfaces that are associated with low activation energy barriers for intercalation/deintercalation. Here, we test this hypothesis by simulating the diffusion of Li ions to the surface and their subsequent deintercalation from the host mesoporous β-MnO_2; molecular graphical anal-

yses[13] of the Li ion trajectories are then used to reveal Li ion deintercalation mechanisms.

METHODS

The Born model of the ionic solid was used to describe β-MnO_2 in which the component Mn and O ions interact via short-range parameterised interactions coupled with long-range Coulombic interactions. The parameters are available in ref [14]. The MD simulations were performed using the DL_POLY code.[15]

Generating Atomistic Models

Structural complexity of nanoporous materials emanates from the synthetic protocol used in their fabrication. Typically, a crystallisation step facilitates the evolution of the polymorphic crystal structure(s) together with microstructural features such as point defects, dislocations, grain-boundaries and (curved) surfaces exposed. Such complexity is difficult to capture within a single atomistic model, but such hierarchical structural features are pivotal if the model is to be used reliably to simulate the properties of the material with sufficient accuracy to benefit experiment. Accordingly, to generate the atomistic models, we have simulated the synthetic protocol – specifically, the crystallisation of MnO_2 starting from amorphous precursors.

Bulk β-MnO_2

To generate an atomistic model of bulk β-MnO_2 a system comprising 8232 manganese and 16464 oxygen ions was first melted and then recrystallized using Molecular Dynamics (MD) simulation. The crystallisation was performed using an NPT ensemble (constant Number of ions, constant Pressure and constant Temperature) at 2000K to ensure the speed of the crystallisation was sufficiently high to facilitate crystallisation within the small timeframe accessible to MD simulation. The latent heat of crystallisation was extracted using a thermostat with relaxation time of 0.1ps.

Mesoporous β-MnO_2

Atomistic models for mesoporous β-MnO_2 we generated by melting a nanoparticle of MnO_2 comprising 24696 atoms and placing the nanoparticle at basis positions of a cubic lattice. The nanoparticle was then agglomerated, under MD simulation, with its periodic neighbours to facilitate a framework architecture; the system was then recrystallized. The strategies used to generate the atomistic models are provided in more detail in ref [16].

Mesoporous Li-MnO_2-β

Models for Li-MnO_2-β, were generated by introducing Li ions into the walls of the atomistic model structure for mesoporous β-MnO_2. Specifically, four models were generated: $Li_{0.03}MnO_2$, $Li_{0.12}MnO_2$, $Li_{0.24}MnO_2$ and $Li_{0.73}MnO_2$, by introducing 250, 991, 2000 and 6000 Li ions respectively into the unit cell of MnO_2. The Li ions were introduced at random sites within the 1x1 tunnels of the host lattice. To maintain charge neutrality, for each Li ion added, an Mn^{4+} ion was reduced (at random positions) to Mn^{3+}. Each model was then equilibrated by performing constant stress MD simulation (NST ensemble: constant Number of ions, constant Stress and constant Temperature) at 300K for 100ps with a preliminary 25ps equilibration step.

Simulating Uniaxial Strain

Strain was imposed upon the unlithiated bulk β-MnO_2, unlithiated mesoporous β-MnO_2 and lithiated mesoporous β-MnO_2 ($Li_{0.03}MnO_2$, $Li_{0.12}MnO_2$, $Li_{0.24}MnO_2$ and $Li_{0.73}MnO_2$) by sequentially increasing the stress along one direction and allowing the system to relax (zero stress) in perpendicular directions using an NST ensemble until the target strain states (1, 2, 3, 4 and 5% strain) were attained. In particular stress increments of 0.01GPa were imposed followed by MD simulation performed at 300K for 5ps. A 5ps equilibration period, was used to help mitigate the effect of the high strain rate.

An additional simulation was also performed on the bulk parent material, fig 1. The stress-strain curve revealed an elastic response to strain up to about 5%. This simulation is somewhat artificial because a bulk ceramic would likely fracture at much lower strains. However, as periodic boundary conditions were imposed there was no surface to enable crack/dislocation propagation; rather this simulation was performed to explore how the system responds to strain when there is no pore space in which to expand/contract.

Simulating Li ion Transport

MD was used to simulate Li-mobility within the host mesoporous MnO_2 including Li transport along the 1x1 tunnels, transport across twin boundaries, transport to the surface, deintercalation from the surface and subsequent transport along the internal surface of the pores. MD simulation was performed for the unstrained, and strained MnO_2. For the strained simulations, +1.6 GPa and -1.6GPa uniaxial stress was imposed to simulate compressive and tensile strain states respectively.

MD simulation was performed for 2ns at 600, 700, 800, 900, 950, 1000, 1050, 1100 and 1150K, using an NST ensemble (constant Number of ions, constant Stress and constant Temperature).

RESULTS

Here, we present the structures of the atomistic models and the structural response when stress is imposed.

Structure: Bulk β-MnO_2

The atomistic structure of the model for bulk β-MnO_2 is shown in fig 1. The model reveals that the MnO_2 has crystallised into the pyrolocite polymorph and comprises a rich microstructure. In particular, fig 1 shows a slice, cut through the bulk MnO_2 revealing dislocations/stacking faults (yellow, blue oval), vacancies (green oval) and microtwinning (red oval). The structure of the molten MnO_2 before crystallisation is shown in fig 1(b).

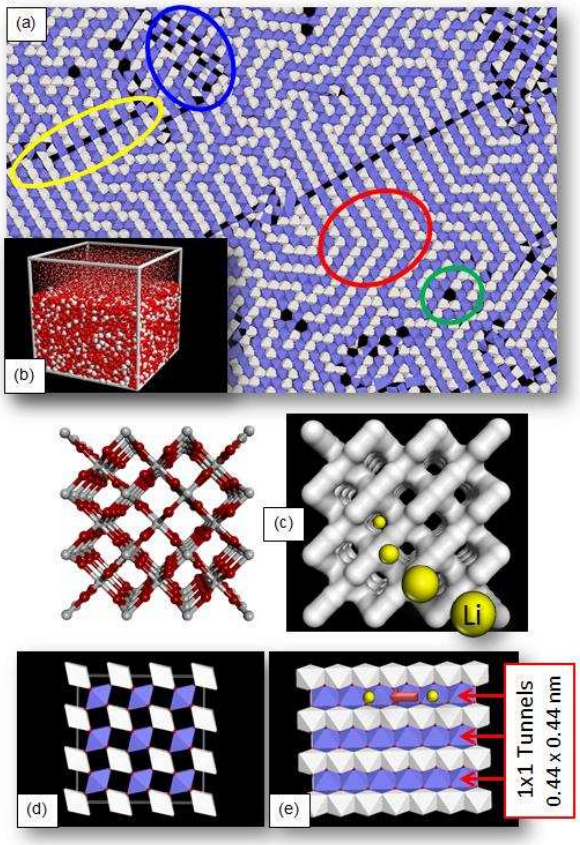

Figure 1 Atomistic model structures for bulk and mesoporous β-MnO_2. (a) Slice cut through the Bulk β-MnO_2 showing the 1x1 tunnels (0.44 x 0.44nm in size) together with a variety of microstructural features. MnO_6 polyhedra are coloured blue and white to better visualise the 1x1 tunnel network. The molten precursor for the bulk structure is shown inset (b) (oxygen is coloured red and manganese, white). (c-e) Crystal structure of MnO_2 conforming to the pyrolucite structure (isostructural with rutile TiO_2). (c, e) illustrate the intercalation of Li ion into one of the 1x1 tunnels. (c) and (d) show views looking along β-MnO_2 [001] where the 1x1 tunnels are perpendicular to the surface, (e) shows a view looking along β-MnO_2 [100].

Structure: Mesoporous β-MnO_2

The atomistic model structure of mesoporous β-MnO_2 is shown in fig. 2. Fig. 2(a) shows a segment of the mesoporous structure revealing the complex interconnecting network of pores. Figs. 2(b,c) show a slice cut through (a) revealing the 1x1 tunnels and microstructural features such as microtwinning (red oval). The microstructure of the mesoporous MnO_2 is therefore commensurate with that of the parent (bulk) material, fig 1(a). Figs. 2(d,e) show the close structural accord between the atomistic model (d) and the real material (e).

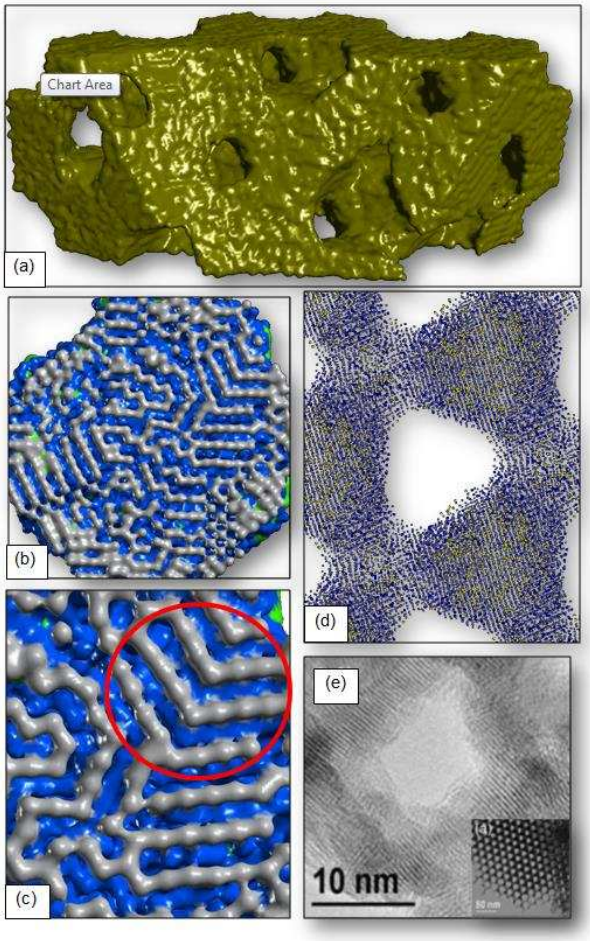

Figure 2 Atomistic model of mesoporous β-MnO_2 compared to experiment. (a) Surface rendered model showing the interconnecting network of pores. (b) Slice cut through the mesoporous MnO_2 showing the 1x1 tunnels. (c) Enlarged segment of (b) showing more clearly microstructural features, such as microtwinning (red oval). (d,e) Experimental validation: (d) Model structure showing one of the pores (e) HRTEM images of real mesoporous MnO_2. Reproduced with permission from ref. [7] Copyright © 2007 WILEY-VCH Verlag GmbH & Co. KGaA, Weinheim.

Uniaxial Stress

The structural response of the mesoporous $Li_{0.24}MnO_2$ to uniaxial stress is shown in fig 3; stress-strain curves for $Li_{0.03}MnO_2$, $Li_{0.12}MnO_2$ and $Li_{0.73}MnO_2$ are presented in supporting information.

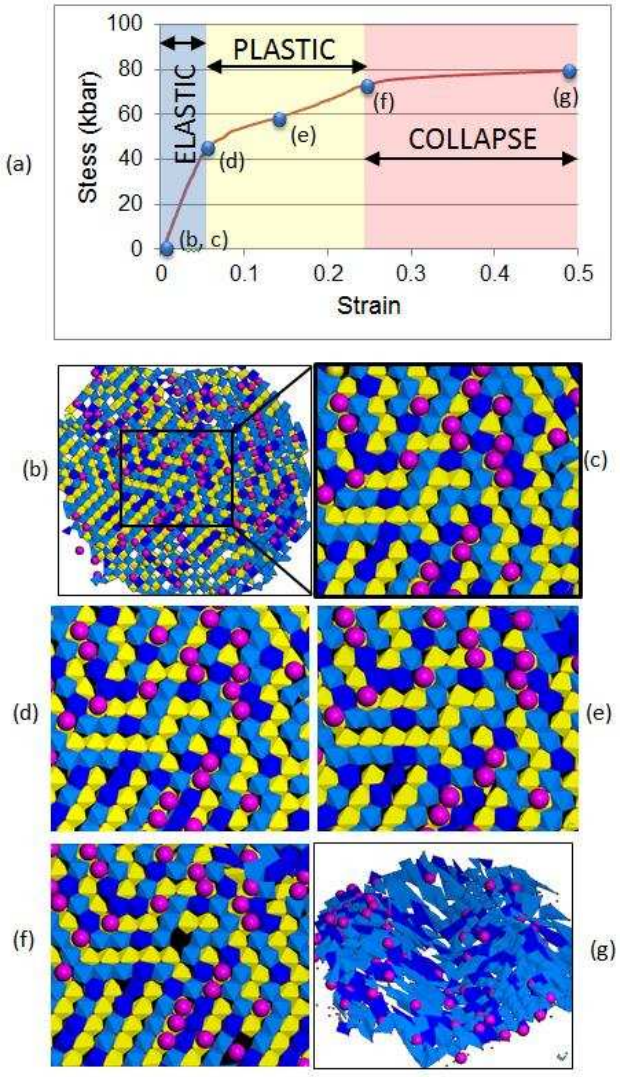

Figure 3 (a) Calculated compressive stress-strain curve for $Li_{0.24}MnO_2$. (b)-(g) slices cut through the mesoporous Li-MnO_2 showing the retention of structural integrity of the 1D tunnels within the walls of the mesoporous material under compression. Images (b-g) correspond to the stress-strain curve (a). (b-d) elastic deformation, (d-f) plastic deformation, (g) structural collapse. Mn^{4+} is coloured light blue, Mn^{3+} is dark blue and Li is pink; manganese surrounded by six oxygen species are represented by polyhedra. The polyhedra coloured yellow correspond to the atomic plane below the blue polyhedra to show more clearly the 1D tunnels and twinning of the MnO_2 host.

After the initial elastic response to stress, the material responds plastically. For the $Li_{0.24}MnO_2$ system, this occurs from about 4-24% strain, fig 3(a). Analysis of the structure during elastic deformation, fig 3(c,d), reveals that the structural integrity of the system is retained with little observable perturbation of the 1x1 tunnels and microstructure, such as twinning. Surprisingly, little structural perturbation is observed during plastic deformation, fig 3(d-f). Finally, the mesoporous structure collapses, fig 3(g), driven by dislocations traversing the structure (as identified using molecular graphical techniques).

Resilience to 24% strain and 7 GPa stress is perhaps unexpected because bulk ceramics normally suffer structural collapse at much lower strains. However, we note that nanostructuring can be used to engineer materials, which can sustain elastic deformation up to 10%,[17] spawning the emerging field of 'ultra-strength' materials.[18] The bulk parent material was also strained by up to 5% to compare with strained mesoporous MnO_2.

Stress-induced structural changes

Li, when intercalated into MnO_2, will induce localised stress upon neighbouring (unlithiated) domains of MnO_2. To act as a host lattice, the MnO_2 must be able to accommodate such stress without collapse of the 1x1 tunnels. Here, we determine how the atomistic structures of bulk and mesoporous MnO_2 change in response to uniaxial stress. In particular, Radial Distribution Functions (RDF) and X-Ray Diffration (XRD) patterns are calculated as a function of uniaxial stress. RDF will capture changes in bond distances and will reveal localised strain within the lattice. Similarly, microstructural changes and tunnel collapse will be reflected in changes to the XRD peak positions.

RDF, calculated for bulk and mesoporous MnO2, are shown in fig 4 and reveal that the 1x1 tunnels in bulk MnO_2 get narrower when the material is compressed, fig 4(a). In particular, peak 3 in fig 4(a), which corresponds to the cross-sectional area of the 1x1 tunnels, broadens and splits as stress is increased. Conversely, when the mesoporous MnO_2 is compressed, fig 4(b), there is no change in the size of the 1x1 tunnels; peak 3 remains unchanged.

XRD patterns, calculated as a function of strain for both bulk and mesoporous MnO_2 are shown in fig. 5. For the bulk material, fig 5(a), the XRD trace changes as a function of strain – the XRD reveals several peaks that split when stress is imposed. Conversely, none of the peaks, associated with mesoporous MnO_2, split as a function of strain, fig 5(b), indicating that the mesoporous MnO_2 is structurally resilient to stress

Molecular graphics was also used to characterise the structures of bulk and mesoporous MnO_2 under uniaxial stress. For bulk MnO2, some of the 1x1 tunnels were compressed such as that shown in fig 6(a,b), which suffered a 9% reduction in size. Fig 6(c,d) shows a 1x1 tunnel in bulk MnO_2 that becomes blocked by Mn under compression, preventing Li transport. In contrast, the size and integrity of the 1x1 tunnels remain unchanged when uniaxial stress is imposed upon the mesoporous MnO_2.

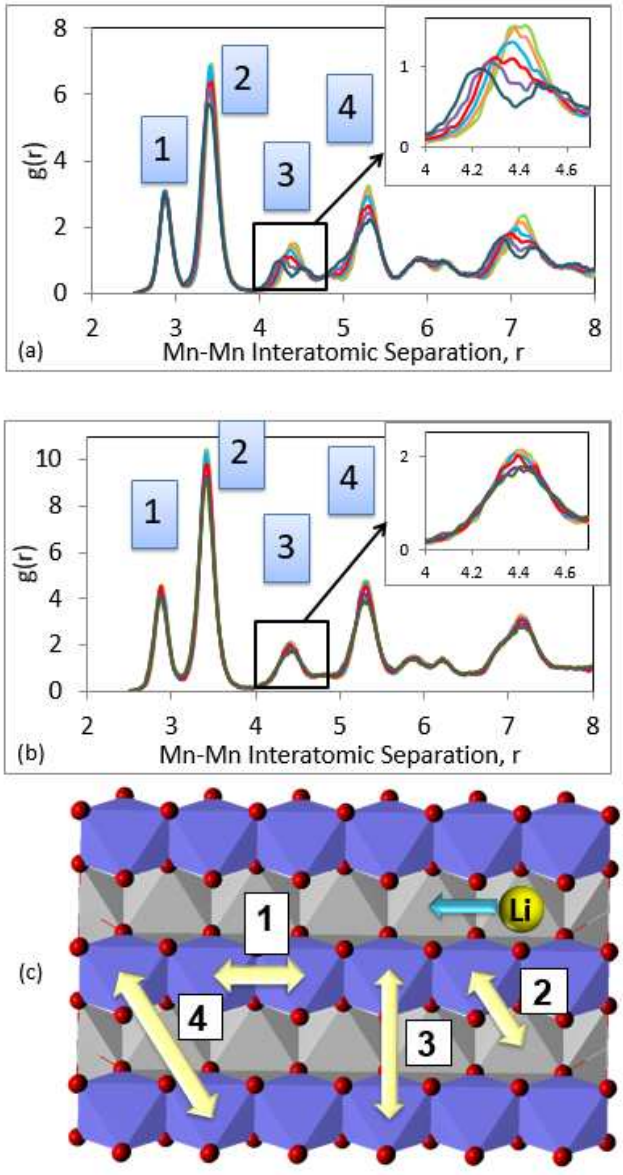

Figure 4 Mn-Mn Radial Distribution Functions, calculated as a function of strain, for (a) bulk and (b) mesoporous β-MnO_2; Mn-Mn distances are in angstroms. (c) Shows how the first four peaks of the RDF (Peak 1, 2, 3 and 4) correspond to the Mn-Mn distances in the β-MnO_2 crystal structure. Peak 1 corresponds to lattice parameter c, and peak 3 corresponds to the lattice parameter a. Colour notation: strain=0% (light green); strain=1% (orange); strain=2% (blue); strain=3% (red); strain=4% (purple); strain=5% (dark green).

Further data and discussion pertaining to the RDF and XRD are reported in supporting information.

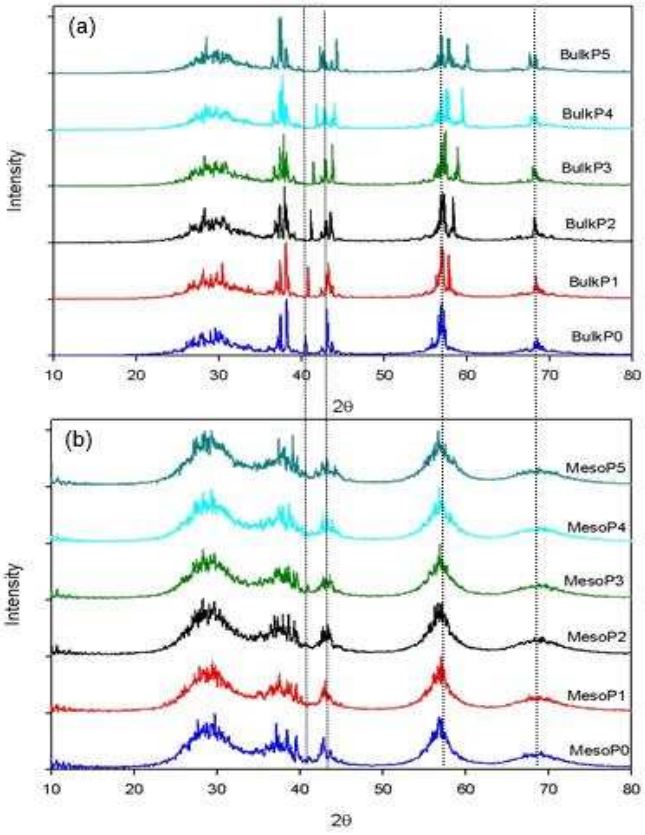

Figure 5 X-ray patterns for (a) bulk β-MnO_2 and (b) mesoporous β-MnO_2, calculated as a function of strain. Labels Po-P5 indicate strains of 0-5% respectively. The dotted lines on the figure indicate the changes in 2θ for the peaks associated with bulk MnO_2 as a function of strain; the XRD trace associated with mesoporous MnO_2 is unchanged.

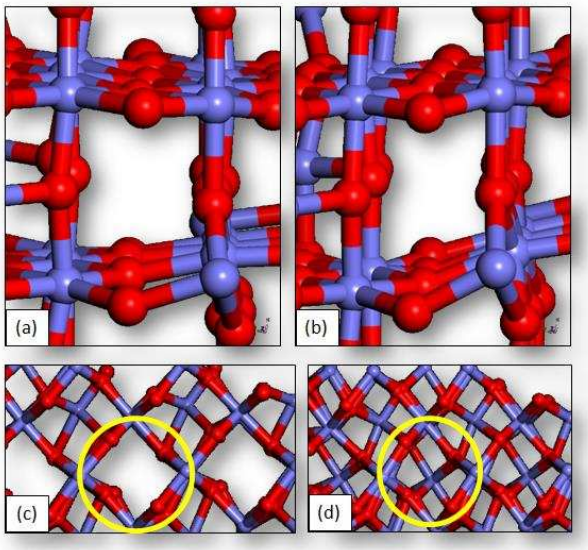

Figure 6 Structure of the 1x1 tunnels in unstrained (a, c) and 5% strained (b, d) bulk β-MnO_2. The structure change (a) to (b) shows a reduction in the size of a 1x1 tunnel and the structural change (c) to (d) shows a 1x1 tunnel that

Li Transport and Deintercalation

During the charging process, Li needs to move through the host lattice to the surface and then deintercalate out of the surface of the host MnO_2 lattice. The structure of the 1x1 tunnels within the host lattice and the 'exit holes' at the surface of the host lattice, through which the Li ions can intercalate and deintercalate, are therefore central to the performance of the battery system. To help understand the structures of the 1x1 tunnels and the entrance/exit holes, the mesoporous MnO_2 model was characterised using molecular graphical techniques and is shown in fig. 7. Analysis of the surface of the internal pores reveals that the entrance/exit holes, for Li intercalation, are not uniform in size or structure, fig 7(c, d), which is attributed to the (concave) curvature of the pores of the material and the multiplicity of crystallographic direction(s) of the 1x1 tunnels in relation to the surfaces of the pores[1].

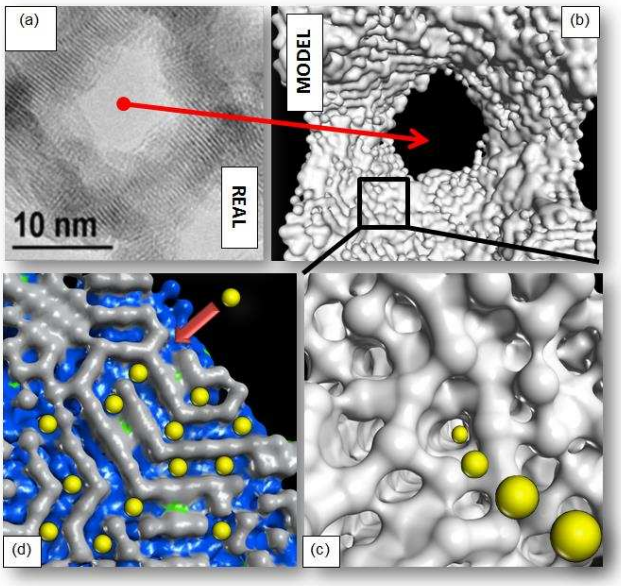

Figure 7 Surface structures of the internal pores in (model) mesoporous β-MnO2. (a) HRTEM image of the real material showing the interconnecting pore structure. (b) Atomistic model showing the interconnecting pore structure. (c) Enlarged segment of (b) showing more clearly the 'entrance' sites in which the Li can intercalate into the MnO2 host lattice (Li is shown as a schematic entering the lattice via one of the entrance sites). (d) Slice cut through the MnO2 showing the 1x1 tunnels in which the Li resides after intercalating into the lattice. (a) Reproduced with permission from ref [7] Copyright © 2007 WILEY-VCH Verlag GmbH & Co. KGaA, Weinheim.

[1] The multiplicity of crystallographic directions with respect to the pores emanates from the considerable microtwinning (see fig 1).

The mobility of Li ions in mesoporous MnO_2 and their subsequent deintercalation from the (internal) pores of the host, was determined by analysing the trajectories of the Li ions during the MD simulations. In particular, Fig 8 shows snapshots, taken during the MD simulation, of a segment of an internal pore. The figure reveals the gradual deintercalation of Li ions from within the host lattice and their subsequent relocation on the surfaces of the internal pores.

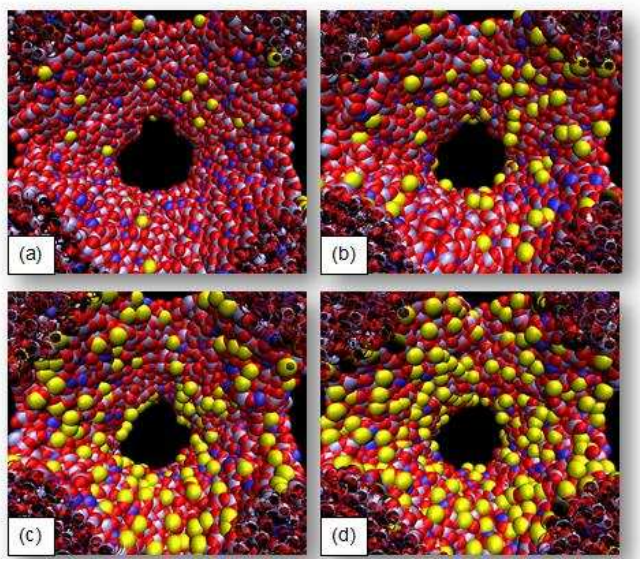

Figure 8 Snapshots, taken during the MD simulation, (a-d), showing the gradual deintercalation of Li out of the host MnO_2 lattice to reside on the (internal) surface of the pore. Li^+ is coloured yellow, O^{2-} is red, Mn^{4+} is grey and Mn^{3+} is blue.

Initially, the Li ions are located 'deep' within the walls of the mesoporous MnO_2 and are accommodated within the 1x1 tunnels of the host, they then diffuse along the 1x1 tunnels, navigating any microtwinning of the structure, to reach the surface prior to intercalating out of the surface via the surface 'exit holes'.

Detailed analysis of the MD trajectory reveals that the deintercallation changes the surface structure of the host MnO2 considerably (fig S7, S8, S9 supporting information).

Transport Energetics

The power and charge time of a Li-ion battery depend upon the energetics associated with Li transport within the lattice and subsequent deintercalation out of the surface of the MnO_2. The activation energy barrier associated with Li-ion mobility and deintercalation was calculated to be 0.41 eV and was extracted from the standard Arrhenius equation, using calculated Mean Square Displacements (MSD). Further details are available as supporting information.

As Li ions intercalate/deintercalate from the host lattice, the strain state of the lattice will change because the Li ions exert stress on the host lattice. Accordingly, we calculated the activation energy barriers, associated with Li ion mobility and deintercallation, for the mesoporous MnO_2 under uniaxial compression (1.6 GPa) and tension (-1.6 GPa) str. Surprisingly, the activation energy barriers do not change when uniaxial stress is imposed: activation energy barriers were calculated to be 0.39 eV (compression), and 0.38 eV (tension), fig 9.

We note that the MSD do not change uniformly with time; rather the MSD trace comprises large fluctuations in the average velocities of the Li ions (fig S11 supporting information). This can be attributed to the variety of processes associated with the Li mobility. These include: the mobility of Li along straight 1x1 tunnels, navigation of Li around twin boundaries and other microstructural defects, the association or binding energy between Li^+ and Mn^{3+} ions, Li arriving at the end of a 1x1 tunnel, deintercalation of the Li from the surface and subsequent diffusion along the (internal) pore surface of the MnO_2. A recent study by Kerisit and co-workers found that the MSD of Li ions within mixed Mn/Ti Oxides show that the MSD is only linear for infinite dilution of Li; the authors attribute such anomalous self-diffusion to Li-Li interactions and association with structural defects.[19]

The equality between the activation energy barriers, calculated for stressed and unstressed MnO_2, are commensurate with data shown in fig. 4 and 5, which show that mesoporous β-MnO_2 mitigates any stress imposed upon it by expanding or contracting into the pore space. Further discussion pertaining to the utilisation of pore space to mitigate stress can be found in supporting information.

Analysis of the model structures during the MD simulations are shown in fig. 9(d-g). The images were generated by superimposing the snapshots taken during the MD simulation. The images reveal that the Li ions are able to move throughout the MnO_2 lattice, via the 1x1 tunnels; the connectivity of the 1x1 tunnels and microtwinning enables all parts of the host lattice to be reached by the Li ions. In particular, fig 9(d, e) shows Li ions at all positions within the lattice. Fig 9(f) shows that once Li has deintercalated out of the surface, it remains mobile on the internal pore surface; Li ions are observed at almost all positions on the internal pore surface. Fig 9(g) reveals that Li transport along the 1x1 tunnels occurs via a hopping mechanism.[20] In particular, the Li ions reside preferentially at the octahedral sites within the 1x1 tunnels, they then hop along the 1x1 tunnel to reside in neighbouring octahedral sites; this is revealed by the dots centred at octahedral sites.

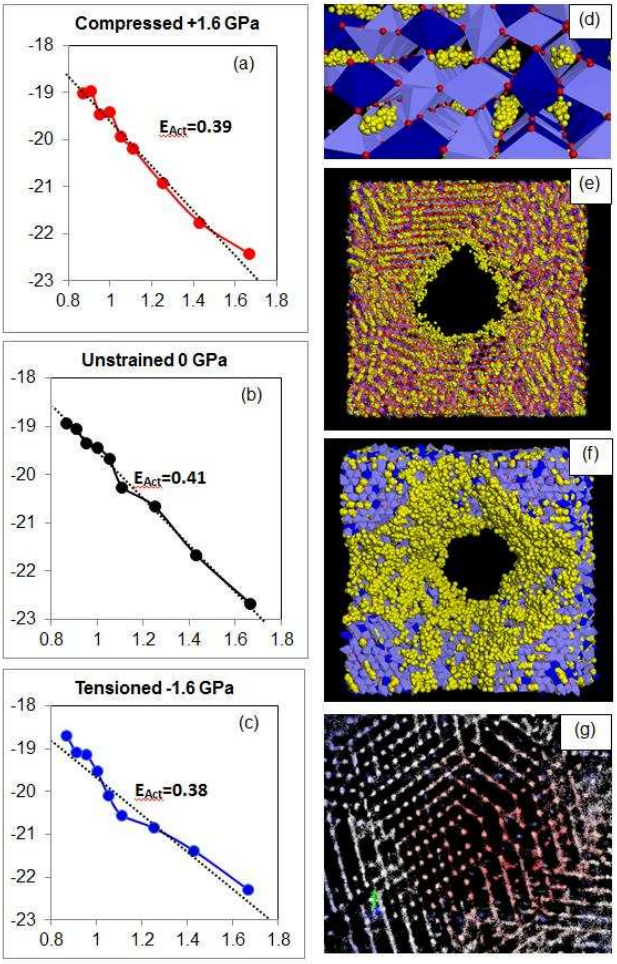

Figure 9 Li ion transport and activation energy barriers, E_{Act}, in stressed and unstressed mesoporous $Li_{0.12}MnO_2$. Li ion diffusion coefficients, LnD_i cm^2/s (ordinate) calculated as a function of inverse temperature K^{-1} (abscissa) for $Li_{0.12}MnO_2$ under (a) +1.6 GPa uniaxial stress, (b) zero stress, (c) -1.6 GPa uniaxial stress. (d-g) structures of $Li_{0.12}MnO_2$ taken during the MD simulations. (d) Li ions occupying positions within the 1x1 tunnels (polyhedral rendering of the MnO_2; Li are represented by yellow spheres). (e) Stick model representation of the MnO_2 host showing Li ions exploring all positions within the 1x1 tunnels throughout the host MnO_2 lattice. (f) Li ions frequenting positions on the surface of the internal pore after they have deintercalated from the lattice. (g) Li ion positions showing that Li ions move along the 1x1 tunnels via a hopping mechanism; Li ions reside primarily within the octahedral sites of the 1x1 tunnels, fig 1(c), coordinated to oxygen prior to hopping to the adjacent octahedral site.

Deintercalation Mechanism

The structure of part of a pore surface comprising mesoporous Li-MnO_2, depicted part way thorough the MD simulation, is shown in fig. 10. Inspection of the figure reveals that Li ions decorate the internal pore surface. Fig 10(b) is an enlarged segment of fig 10(a) revealing three Li ions (labelled 1, 2 and 3) that lie just under the surface of the pore. At a later stage of the MD simulation, each of the three Li ions can be seen to have deintercalated from the MnO_2 and reside on the surface of the pore, fig 10(c).

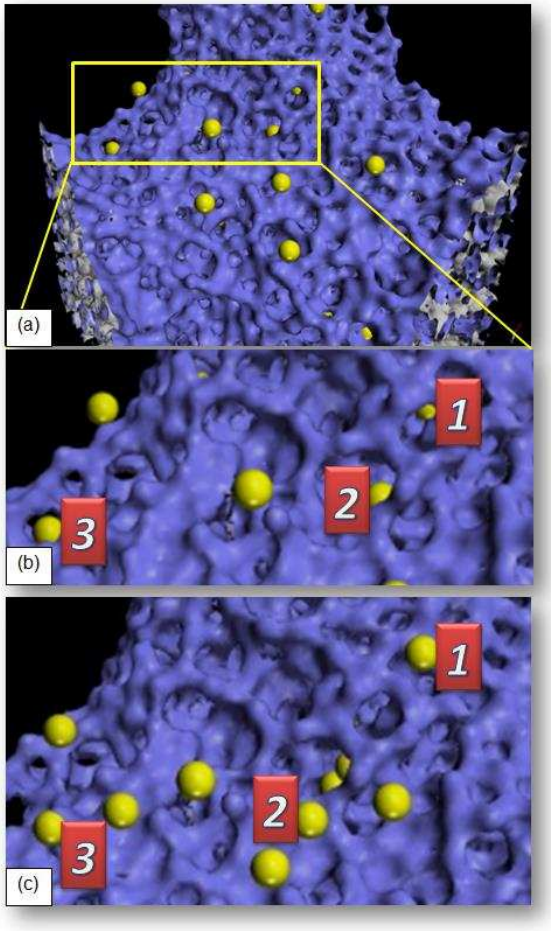

Figure 10 (a) Segment of the surface of a pore within the mesoporous MnO_2 shown part way through the MD simulation after a number of Li ions have deintercalated out of the MnO_2. An enlarged segment of (a) is shown in (b). (c) is the same as (b) but after a few more cycles of MD simulation showing Li that has moved from just inside the surface (b), to just outside the surface (c). Labels 1,2 and 3 help identify the particular Li ion that deintercalates. Li is coloured yellow, mesoporous MnO_2 is shown using surface rendering.

The MD trajectory of an individual Li ion was then tracked to elucidate how it deintercalated from the surface. Initially, the Li ion is located within one of the 1x1 tunnels, fig 11(a). It then traverses along this 1x1 tunnel towards the surface. However, rather than deintercalate out of the end of the 1x1 tunnel, the Li-ion deintercalates out of the *side* of the 1x1 tunnel along [001] as indicated by the white arrow on fig 11(a). The Li then exits via an opening at the surface bounded by five MnO_2 octahedra, fig 11(b): First it becomes level with the surface, fig 11(c) and then proceeds to diffuse along the surface of the pore, fig 11(d). We note that as the Li moves through the tunnel the atomistic configuration of the tunnel changes, as evidenced by inspection of figs 11(b-d). The sizes and shapes of the exit/entrance sites do not only show a wide variety of structural configurations, but also change dynamically, which we attribute to the reduction in strain state of the host MnO_2 as Li deintercallates.

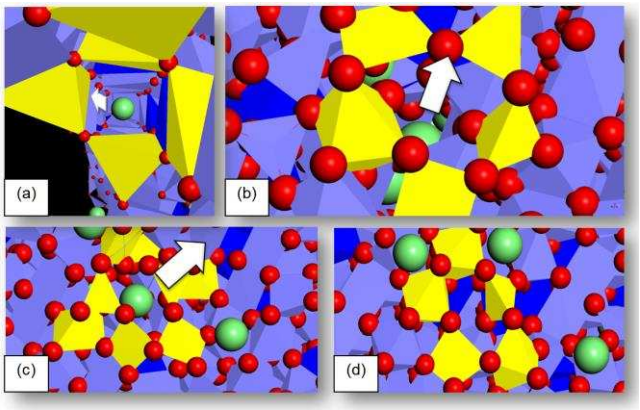

Figure 11 Snapshots taken during the MD simulation showing a Li ion deintercalating out of the surface of the MnO_2. (a) Li located just inside the mesoporous Li-MnO_2-β, (b) Li level with the surface of the MnO_2 pore, (c) Li just outside the surface, (d) Li migration along the surface of the MnO_2 pore.

DISCUSSION

Here we summarise the key findings of the influence of stress, associated with Li intercalation, on the size and structural integrity of the 1x1 tunnels within bulk and mesoporous β-MnO_2. We next summarise how Li intercalates/deintercalates from bulk and mesoporous β-MnO_2.

Mechanical resilience to stress

Bulk β-MnO_2

- Compressive stress changes the structure and dimensions of the 1x1 tunnels, perturbs the microstructure and blocks the 1x1 tunnels.

Mesoporous β-MnO_2

- Compressive stress does not perturb the microstructure and no changes to either the structure or dimensions of the 1x1 tunnels are observed.

Li Intercalation/Deintercalation

Bulk MnO_2

- The calculated activation energy barrier, associated with Li deintercalation from a perfect (101) surface of the bulk material, is >0.6eV, 'which is likely to preclude their practical use'.[21]

Mesoporous β-MnO_2

- The calculated activation energy barrier, associated with Li-ion transport to the pore surface and subsequent deintercalation from mesoporous MnO_2, is calculated to be about 0.4 eV
- The, 0.4eV, activation energy barrier is irrespective of whether the host lattice is in an unstrained, compressive (1.6GPa) or tensive (-1.6GPa) strain state.
- High-curvature porous nanostructuring facilitates a wide variety of 'exit-hole' sizes and atomistic configurations through which the Li can intercalate/deintercalate in contrast to the parent bulk material.

Experimentally, Ren and Bruce found that the (thin) walls of the mesoporous β-MnO_2 can accommodate the stress associated with the phase boundary between β-MnO_2 and Li_xMnO_2-β despite the large volume expansion on intercalation (unit cell: 55.7 to 72.3 $Å^3$) and its significant anisotropy (β-MnO_2: a = 4.406 Å, c = 2.868 Å; Li_xMnO_2-β: a = 5.141 Å, b= 5.002 Å, c = 2.813 Å).[22] Our simulations rationalise this ability of the mesoporous material. In particular, akin to Le Chatalier's principle, the mesoporous material mitigates the effect of stress, associated with the phase boundary between β-MnO_2 and Li_xMnO_2-β, by expanding or contracting into the void space of the mesoporous material. In particular, we propose the concept of mesoporous 'breathing-crystals' in which the nanomaterial is able to expand and contract *elastically*, in response to stress, without influencing its structural integrity.

Moreover, we proffer that such breathing-crystal response to stress is a phenomenon associated with mesoporous materials in general. In particular, previous studies have shown that nanomaterials can accommodate high levels of strain without suffering plastic deformation spawning the field of strain-engineering,[23] where physical (ionic conductivity,[24] band structure[25]) chemical (activity[26]) and mechanical (ultra-strength materials[27,28]) properties can be tuned by altering the strain state.

Our findings epitomise the need to have models, which capture the structural complexity of the real material. This includes: the atomistic structure and connectivity of the network of pores, the exit holes through which the Li ions intercalate and deintercalate from the material and the microstructure of the material (microtwinning and connectivity of the 1x1 tunnels, (point) defects, dislocations and more general grain-boundaries). Moreover, to simulate the diffusion process, where the mobility of Li is likely concerted, a high number of Li ions must be included within a single simulation cell to capture the diverse range of correlated mechanisms associated with Li mobility. At present, the number of atoms required to capture all these features within a single model is too large to be considered quantum mechanically (using for example, density functional theory) and therefore atomistic simulation, using pair potentials, continues to provide a valuable tool to be used in conjunction with quantum mechanical methods; together they provide unique insight for experiment.

CONCLUSION

Molecular Dynamics simulation has been used to generate atomistic models of bulk and mesoporous MnO_2, which comprise a rich microstructure including: microtwinning, point defects (vacancies), dislocations and grain-boundaries. We use the models to show that compressive stress in mesoporous β-MnO_2 (emanating from Li intercalation) does not influence the structure or dimensions of the 1x1 tunnels in which the lithium ions intercalate, reside and deintercalate. Conversely, compressive stress imposed upon bulk β-MnO_2 changes the structure and size of the 1x1 tunnels and results in blocking of some of the tunnels rendering the bulk parent material electrochemically inactive. We propose that nanostructuring facilitates 'breathing-crystals', where the material is able to mitigate the effect of stress, and retain its structural integrity, by relaxing elastically into the pores.

Moreover, the network of pores within mesoporous β-MnO_2 comprise curved surfaces, which facilitate a wide variety of sizes and structural configurations of 'exit sites' for Li deintercalation in contrast to the parent bulk material. We simulate directly the transport of Li ions to the (curved pore) surfaces of the host mesoporous β-MnO_2 lattice and their subsequent deintercalation out of the surfaces via these exit sites and calculate an activation energy barrier of 0.4eV; the activation energy barrier does not change even when the mesoporous Li-MnO_2 is under compressive (1.6GPa) or tensile (-1.6GPa) stress. Our simulations also reveal that the atomistic structures of the 'exit sites' change dynamically as Li deintercalates.

ACKNOWLEDGEMENT

South African Research Chair Initiative of the Department of Science and Technology, and the National Research Foundation.

AUTHOR INFORMATION

Corresponding Author

* Dean C. Sayle d.c.sayle@kent.ac.uk

Table of contents artwork

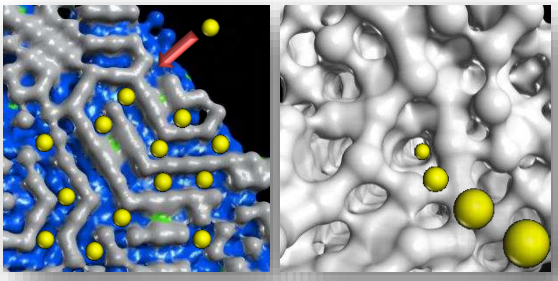

REFERENCES

[1] Uchaker, E. and Cao, G.R.
Mesocrystals as electrode materials for lithium-ion batteries
Nano Today , 2014, 9, 499

[2] Chabre, Y and Parmetier, J.
Structural and electrochemical properties of the proton Y-MnO_2 system.
Prog. Solid. St. Chem. 1995, 23, 1.

[3] Luo, J. Y.; Zhang, J. J. and Xia, Y. Y.
Highly Electrochemical Reaction of Lithium in the Ordered Mesoporosus β-MnO2
Chem. Mater. 2006, 18, 5618

[4] Bruce, P. G.; Scrosati, B. and Tarascon, J. M.
Nanomaterials for Rechargeable Lithium Batteries
Angew. Chem. Int. Ed. 2008, 47, 2930

[5] Islam, M. S. and Fisher, C. A. J.
Lithium and sodium battery cathode materials: computational insights into voltage, diffusion and nanostructural properties
Chem. Soc. Rev., 2014, 43, 185

[6] Wang, D.; Liu, L.M.; Zhao, S.J; Li, B.H.; Liu, H. and Lang, X.F.
Beta-MnO_2 as a cathode material for lithium ion batteries from first principles calculations
Phys. Chem. Chem. Phys. 2013, 15, 9075

[7] Jiao, F. and Bruce, P.G.
Mesoporous Crystalline β-MnO_2—a Reversible Positive Electrode for Rechargeable Lithium Batteries
Adv. Mater. 2007, 19, 657

[8] Huang, J.Y.; Zhong, L.; Wang, C.M.; Sullivan, J.P.; Xu, W.; Zhang, L.Q.; Mao, S.X.; Hudak, N.S.; Liu, X.H.; Subramanian, A.; Fan, H.Y.; Qi, L.A.; Kushima, A. and Li, J.
In Situ Observation of the Electrochemical Lithiation of a Single SnO_2 Nanowire Electrode
Science, 2010, 330, 1515

[9] Zhang, L.Q.; Liu, X.H; Liu, Y; Huang, S.; Zhu, T; Gui, L.J.; Mao, S.X.] ; Ye, Z.Z.; Wang, C.M.; Sullivan, J.P. and Huang, J.Y
Controlling the Lithiation-Induced Strain and Charging Rate in Nanowire Electrodes by Coating
ACS Nano 2011, 5, 4800

[10] Ramadesigan, V.; Northrop, P. W. C.; De, S.; Santhanagopalan, S.; Braatz, R. D. and Subramanian, V. R.
Modeling and Simulation of Lithium-Ion Batteries from a Systems
J. Electrochem. Soc. 2012, 159, R31

Engineering Perspective
[11] Tompsett, D. A.; Parker, S. C. and Islam, M. S.
Rutile β-MnO2 Surfaces and Vacancy Formation for High Electrochemical and Catalytic Performance
J. Am. Chem. Soc. 2014, 136, 1418

[12] Dawson, J. A. and Tanaka, I.
Li Intercalation into a β-MnO2 Grain Boundary
ACS Appl. Mater. Interfaces 2015, 7, 8125

[13] Humphrey, W., Dalke, A. and Schulten, K.,
VMD - Visual Molecular Dynamics
J. Molec. Graphics, 1996, 14, 33

[14] Sayle, T.X.T., Maphanga, R.R., Ngoepe, P.E. and Sayle, D.C.
Predicting the Electrochemical Properties of MnO_2 Nanomaterials Used in Rechargeable Li Batteries: Simulating Nanostructure at the Atomistic Level
J. Am. Chem. Soc., 2009, 131, 6161

[15] Smith, W., and Todorov, I. T.
A short description of DL_POLY
Mol. Simul., 2006, 32, 935

[16] Sayle, D.C.; Seal, S.; Wang, Z.; Mangili, B.C.; Price, D.W.; Karakoti, A.S.; Kuchibhatla, S.V.T.N.; Hao, Q.; Möbus, G.; Xu, X. and Sayle, T.X.T.
Mapping Nanostructure: A Systematic Enumeration of Nanomaterials by Assembling Nanobuilding Blocks at Crystallographic Positions
ACS Nano., 2008, 2, 1237

[17] Shan, Z. W.; Adesso, G.; Cabot, A.; Sherburne, M. P.; Asif, S. A. S.; Warren, O. L.; Chrzan, D. C.; Minor, A. M. and Alivisatos, A. P.
Ultrahigh stress and strain in hierarchically structured hollow nanoparticles
Nat. Mater., 2008, 7, 947

[18] Suresh, S. and Li, J.
Materials Science Deformation of the ultra-strong
Nature, 2008, 456, 716

[19] Kerisit, S.; Chaka, A.M; Droubay, T.C. and Ilton, E.S.
Shell Model for Atomistic Simulation of Lithium Diffusion in Mixed Mn/Ti Oxides
J. Phys. Chem. C, 2014, 118, 24231.

[20]Wang, D.; Liu, L. M.; Zhao, S. J.; Li, B. H.; Liu, H. and Lang, X. F.
β-MnO2 as a cathode material for lithium ion batteries from first principles calculations
Phys. Chem. Chem. Phys., 2013,15, 9075

[21] Tompsett, D.A.; Parker, S. C.; Bruce, P.G. and Islam, M. S.
Nanostructuring of β-MnO_2: The Important Role of Surface to Bulk Ion Migration
Chem. Mater. 2013, 25, 536

[22] Ren, Y.; Armstrong, A.R.; Jiao, F. and Bruce, P.G.
Influence of Size on the Rate of Mesoporous Electrodes for Lithium Batteries
J. Am. Chem. Soc. 2010, 132, 996

[23] Paskiewicz, D. M.; Scott, S. A.; Savage, D. E.; Celler, G. K. and Lagally, M. G.
Symmetry in Strain Engineering of Nanomembranes: Making New Strained Materials
ACS Nano, 2011, 5, 5532

[24]Wen, K.; Lv, W. and He, W.
Interfacial lattice-strain effects on improving the overall performance of micro-solid oxide fuel cells
J. Mater. Chem. A, 2015, Advance Article; DOI: 10.1039/C5TA03009A

[25]Smith, A. M.; Mohs, A. M. and Nie, S.
Tuning the Optical and Electronic Properties of Colloidal
Nanocrystals by Lattice Strain
Nat. Nanotechnol. 2009, 4, 56.

[26]Sayle, T. X. T.; Cantoni, M.; Bhatta, U. M.; Parker, S. C.; Hall, S. R.; Möbus, G.; Molinari, M.; Reid, D.; Seal, S. and Sayle, D. C.
Strain and Architecture-Tuned Reactivity in Ceria Nanostructures; Enhanced Catalytic Oxidation of CO to CO2
Chem. Mater., 2012, 24, 1811

[27]Zheng, X.; Lee, H.; Weisgraber, T. H.; Shusteff, M.; DeOtte, J.; Duoss, E.B.; Kuntz, J. D.; Biener, M. M.; Ge, Q.; Jackson, J. A.; Kucheyev, S. O.; Fang, N. X. and M. Spadaccini, C. M.
Ultralight, ultrastiff mechanical metamaterials
Science 2014, 344, 1373

[28] Zhu, T. and Li, J.
Ultra-strength materials
Prog. Mater. Sci. 2010, 55, 710.